Visual Field Inhomogeneities and the Architectonics of Early Visual Cortex shape Visual Working Memory

Julia Papiernik-Kłodzińska[1,2,3], Simon Hviid Del Pin[4], Kristian Sandberg[5,6], Michał Wierzchoń[1,3], Marisa Carrasco[7], & Renate Rutiku[1,3*]

[1] Consciousness lab, Institute of Psychology, Jagiellonian University, Krakow, Poland
[2] Doctoral School in the Social Sciences, Jagiellonian University, Krakow, Poland
[3] Centre for Brain Research, Jagiellonian University, Krakow, Poland
[4] Norwegian University of Science and Technology, Gjøvik, Norway
[5] Center of Functionally Integrative Neuroscience, Aarhus University and Aarhus University Hospital, Universitetsbyen, Aarhus, Denmark;
[6] Neurobiology Research Unit, Copenhagen University Hospital Rigshospitalet, Copenhagen, Denmark;
[7] Department of Psychology and Center for Neural Science, New York University

Email: renate.rutiku@uj.edu.pl

Abstract

Whether early visual cortex (V1) is essential for visual working memory (vWM) performance remains a topic of scientific debate. The current study aimed to expand previous research findings by examining whether idiosyncratic structural properties of V1, particularly visual field inhomogeneities such as visual field and polar angle asymmetries, are reflected in interindividual differences in vWM performance. A total of 292 participants underwent an MRI scan using a multiparametric mapping sequence, generating four quantitative microstructural maps per participant: magnetization transfer (MT), proton density (PD), longitudinal relaxation rate (R1), and transverse relaxation rate (R2*). In a separate session, the participants completed a vWM task designed to probe visual field inhomogeneities. Behavioral results are consistent with previously reported asymmetries in vWM, particularly the inverted polarity of the vertical meridian asymmetry (VMA). Quantitative MRI analysis revealed associations between VMA and multiple qMRI parameters in V1, indicating that individual differences in V1 architecture contribute to variability in vWM performance. Additionally, cortical thickness measures revealed a link between V3 and left–right asymmetry, suggesting that structural variability beyond V1 also shapes vWM performance. These findings are consistent with the sensory recruitment hypothesis and suggest that structural characteristics of early visual areas influence vWM performance.

Keywords: Polar angle asymmetries, Visual working memory, Multiparametric mapping, V1, Quantitative MRI, Sensory recruitment hypothesis

Introduction

Working memory is the core ability of our minds to "hold a limited amount of information temporarily in a heightened state of availability for use in ongoing information processing" (Definition 6 in Cowan, 2017). Consequently, the term 'visual working memory' (vWM) is used to specifically denote the temporary storage and use of visually perceived information (Lorenc, Mallett & Lewis-Peacock, 2021). It is known that vWM is severely limited in capacity, and interindividual differences in capacity limits are strongly linked to other aspects of cognitive ability such as intelligence (Fukuda et al., 2010). For this reason, there is a lot of interest in why people with otherwise comparable perceptual abilities can differ so markedly in terms of how well they are able to retain the perceived information over time (Luck & Vogel, 2013). The two hallmarks of vWM – its small capacity and the stable interindividual differences have also been instrumental in guiding the search for the neural underpinnings of vWM ability.

Due to the sparse nature of working memory in general, it was originally thought that separate modality-specific working memory storages exist away from the high-capacity sensory cortices with their rich perceptual representations. It was theorized that perceptual contents are first encoded into more abstract representations and subsequently retained in the frontal (and/or parietal) cortices. Indeed, the landmark monkey study by Funahashi and colleagues (1989) delivered compelling evidence for such a theoretical model (see also Miller et al., 1996). This separation between perception and vWM retention was put into question by Harrison & Tong (2009) and Serences and colleagues (2009), however, by demonstrating that the content of vWM can also be tracked in the primary visual cortex (V1). Many studies followed with similar findings (see Christophel et al., 2017 and Ma et al., 2014 for reviews), leading to the proposition of the sensory recruitment model. This model suggests that early sensory areas are involved in maintaining modality-specific information in working memory, leveraging existing specialized neural circuits for efficient temporary storage of detailed sensory input (Adam et al., 2022). Despite the intuitive appeal of the sensory recruitment model, however, it is still controversial whether vWM relies on the same neural substrate as visual perception or not, with strong empirical evidence on both sides of the debate (see Sheremata et al., 2023 and Zhao et al., 2022 for support, and Bettencourt & Xu, 2016 and Iamshchinina et al., 2021 for critique; see also Tardiff & Curtis, 2025, for review).Given that the interindividual differences in vWM capacity are quite stable over time (Hockey & Geffen, 2004; Johnson et al., 2013) it stands to reason that there also exist stable interindividual differences in brain structure underlying the behavioral effects. This offers a unique opportunity to use the varying vWM tasks performance limits among people to uncover their neural origin (i.e. a correlational approach instead of the experimental approach; Cronbach, 1957; Hedge et al., 2018). Focusing on the aspects of behavior that exhibit meaningful differences among people also

helps to potentially overcome some caveats of the experimental study designs (where the focus is on differences between conditions/trials not among individuals) such as confounding the neural correlates of vWM with correlates of other task-related processes. A number of studies have already employed the interindividual-differences approach to identify the neural basis of vWM performance limits with varied results.

On the one hand, initial evidence demonstrates a link between vWM performance and specifically V1 structure (Bergmann et al., 2016). Thirty-one participants were tested on a delayed Gabor patch orientation discrimination task. Participants' performance on this task was strongly linked to their individual V1 gray matter volume, whereas no similar correlations were found for extrastriatal visual cortex or higher-order areas via whole-brain analyses. On the other hand, using a combination of two visual tasks – one focusing on spatial vWM and the other on vWM of object identity – resulted in no link with V1 structure for either task (n=48). Instead, the spatial task was linked to gray matter volume in the inferior parietal lobules and the object identity task was linked to gray matter volume in the insulae (Konstantinou et al., 2017). Moreover, testing thirty-two participants on two typical visuospatial memory tasks revealed a strong link between total brain volume and behavioral performance. When this association with total brain volume was accounted for, none of the local correlations in V1 and intraparietal sulcus were significant anymore (even though moderate correlations were evident if total brain volume was not accounted for; Dimond et al., 2018). Finally, an entirely different approach compared to the typical regions-of-interest (ROI) analysis was taken, involving the training of machine learning models on a large multimodal MRI dataset (n=547) with hundreds of thousands of features to predict individual vWM capacity scores on a task including colored dots. The findings revealed widespread associations with behavioral performance across the entire brain. The strongest model weights were found within the motor network and the subcortical-cerebellum network whereas links within the early visual cortex were weak to absent (Xiao et al., 2021) .

In summary, previous studies point to various areas where gray matter volume seems to account for behavioral differences in vWM tasks (whereas no noteworthy links with white matter structure have been reported). Yet the findings do not provide a clear answer as to whether V1 is involved in vWM performance or not. The heterogeneity of the findings may be influenced by several factors. For example, the stimulus material within each study tends to be quite limited whereas the stimulus material across studies varies widely. Whereas this is not necessarily a shortcoming (as WM is often thought to be very domain-specific and may differ, for example, between spatial vWM and object-based vWM; see Konstantinou et al., 2017) it does make it less likely that common neural markers are identified across studies. A potentially more serious methodological problem is posed by

the fact that many brain-behavior correlation studies - including ROI-based studies - to date may have been underpowered (for a discussion, see Dubois & Adolphs (2016), Marek et al. (2022), Gratton et al. 2022) and Rosenberg & Finn (2022)). Depending on the stability and robustness of the behavioral effects, brain-wide association studies should include upwards of a couple hundred participants in order to detect replicable findings (Kang et al., 2024). Many, if not all, behavioral effects include significant sources of noise with respect to the psychological constructs of interest because they are a product of many cognitive processes acting in unison to produce the measured outcome. It is safe to assume that the behavioral estimation of vWM performance limits in the studies cited above also include such measurement error stemming from the nature of the tasks and the type of behavioral effects that the tasks were optimized for. Therefore, in order to maximize the sensitivity of a study, the relevance of any behavioral effect with respect to the actual latent construct of interest should be carefully considered. Ideally, the behavioral effect would not only be maximally sensitive to the psychological constructs of interest but also to the difference between alternative hypotheses.

For example, if interindividual differences in vWM performance are indeed to some extent a consequence of structural V1 differences, then vWM performance should also exhibit other consequences that mirror the structural properties of V1. If V1 is not involved, then vWM should not be influenced by the structural idiosyncrasies of V1 (and the behavioral consequences thereof). The most striking structural property of V1 is of course its retinotopy and the cortical magnification factor for foveal vision. Indeed, it is implicitly assumed that this is the reason why V1 volume might be linked to vWM performance. To put it simply, more cortical real estate affords more storage similar to having a larger and more precise map (Jeong, 2023). However, V1 structure is also marked by another important idiosyncrasy, namely its inhomogeneous representation of the visual field. As described in a review by Karim & Kojima (2010) the visual field inhomogeneities include phenomena such as the differences between left and right or upper and lower visual field performance, with lower visual field dominating in a wide variety of tasks, (including e.g. contrast pattern recognition, perception of color changes or motion perception).

Some authors have highlighted that the upper versus lower field effect in contrast sensitivity and acuity tasks is primarily driven by the vertical meridian, and accordingly has been described as the vertical meridian anisotropy (VMA). This is accompanied by an even stronger effect known as the horizontal-vertical anisotropy (HVA), i.e., the dominance of performance along the horizontal compared to the vertical meridian of the visual field (review, Himmelberg, Winawer & Carrasco, 2023). Those two phenomena are known as polar angle asymmetries. It should be noted that even though the polar angle asymmetries are already present in the organization of the photoreceptors and retinal-ganglion cells (Curcio et al., 1990; Curcio & Allen, 1990; Song et al., 2011; Watson, 2014),

these retinal factors only partially explain the observed behavioral effects, pointing to the role of V1 (Kupers et al., 2019 and 2022), which manifests the polar angle asymmetries both in brain structure (Benson et al., 2021; Himmelberg et al., 2023) and function (Himmelberg et al., 2022; Kurzawski et al., 2022; Liu et al., 2006; O'Connell et al., 2016). In the following, we will use the term 'visual field inhomogeneities' when referring to both polar angle asymmetries and visual field asymmetries together.

If V1 is involved in vWM performance, it should be possible to detect asymmetries in the performance of vWM tasks across the visual field and/or polar angles. Behavioral evidence that this is indeed possible has already been reported. A 2009 study examining spatial frequency discrimination and perceived spatial frequency in visual short-term memory tasks demonstrated that both horizontal (HVA) and vertical (VMA) visual field asymmetries extend to performance in spatial frequency discrimination tasks, in both the two-alternative forced choice and two-interval forced choice variants. (Montaser-Kouhsari & Carrasco, 2009). Visual field asymmetries in vWM performance have been also reported by Del Pin et al. (2020), authors used the typical two-alternative forced choice object-identification vWM task with a retro cue and eight target locations equally spaced on a circular display on a sample of 43 volunteers. Participants had to identify the target object at the cued location and rate its visibility on the 4-point Perceptual Awareness Scale (Overgaard, Rote, Mouridsen, & Ramsøy, 2006). Both identification accuracy and visibility ratings exhibited two clear asymmetry patterns across the memory array. The most prominent pattern closely resembled a typical HVA. An asymmetry was also present along the vertical axis similar to VMA, albeit with an untypical direction – performance was on average better for the upper location compared to the lower locations.

These behavioral results offer compelling evidence for the potential involvement of V1 in vWM because they reveal that vWM performance exhibits a pattern of visual field inhomogeneity that is most characteristic of V1. The goal of the present study was to replicate the behavioral findings of Del Pin et al. (2020) in a representative sample for interindividual differences research, assess whether the unusual inverted VMA pattern is robust, test whether the asymmetry patterns link to interindividual differences of V1 structure, and identify potential underlying tissue properties within V1 that might explain any connection between brain structure and task performance. We also attempt to conceptually replicate the results of Bergmann and colleagues (2016) and complement their findings related to V1 surface area with a volumetric analysis of the potential underlying tissue properties.

Methods

Participants

This study was conducted as part of the EU COST Action CA18106 (www.neuralarchcon.org), at the data collection site in Kraków (Consciousness Lab, Jagiellonian University, Kraków, Poland). The broader consortium project includes an extensive behavioral test battery, MRI, EEG, and DNA probing of neurotypical participants. The current study focuses exclusively on one visual working memory task within the larger behavioral battery and links it to interindividual variation specifically in the neuroarchitectural characteristics.

A total of 292 participants (185 F and 107 M), aged 18 to 40.9 years old, (mean = 23,9; SD = 4,47) took part in the study. The sample size has been adjusted to hold sufficient power after the correction for multiple comparisons that is used in whole-brain analyses. For details see Section 1.3.2 of the Technical Annex of the Action (COST, 2018). The participants were physically healthy at the time of assessment, had normal or corrected-to-normal vision, and normal hearing. They did not have a history of brain damage or brain surgery, nor any known brain abnormalities, and did not use neuropharmacological or other medication that may affect neural states. Additionally, the exclusion criteria included pregnancy, skin diseases and bodily build that would not allow for an MR scan. All participants also complied with the standard MRI safety criteria and signed the respective informed consent forms in order to participate in the project. The project complies with the Declaration of Helsinki and was approved by the ethical committee at the Institute of Psychology, Jagiellonian University.

Participants attended two separate sessions for this study. During the first one, they underwent multiparametric mapping (MPM; Weiskopf, 2013) MRI scan (among other MRI sequences) and during the second session, they performed the visual working memory task (among other behavioral tasks also performed in the same session). The two sessions were separated by 11 days on average (sd = 6.6, range = 2 to 40).

Behavioral task

The visual working memory task in this study was similar to the object recognition task designed by Del Pin and colleagues (Del Pin et al., 2020). The task was created using the Psychopy Toolbox (Peirce et al., 2019), and comprised 256 trials, each containing the following sequence: The fixation cross, designed by Thaler and colleagues (2013) to improve the stability of the fixation, was presented throughout the trial, except during the response screen Next, eight images of objects, enclosed in squares with black outlines, were presented on the screen in a circular array centered at 6.8 degrees eccentricity around the fixation cross. After 1000 ms, the images of objects disappeared, but the black squares remained on the screen as location placeholders until the response screen. 100 ms after the

stimuli had disappeared, a cue was presented for 500 ms. The cue consisted of a black line pointing to one of the 8 locations. Finally, after 1400 ms an image of an object appeared in the center of the screen. The participants had to answer if this was the same exact object that had been presented in the cued location or not. The schematic representation of the trial structure is presented in **Figure 1A**.

A set of 200 images (approximately 60% depicting manmade and 40% natural objects; no two images depicting the same object) was selected from the Snodgrass and Vanderwart *Like* object repository (Rossion & Pourtois, 2004). A subset of the images is available in SI1. The stimuli were chosen based on the ease of naming the depicted objects in Polish, ensuring that participants could recognize them without difficulty. The objects were of similar size with respect to the enclosing squares while still maintaining clear gaps between the image and the borders of the square, but not controlled for their low-level properties (such as color, orientation, or spatial frequency).

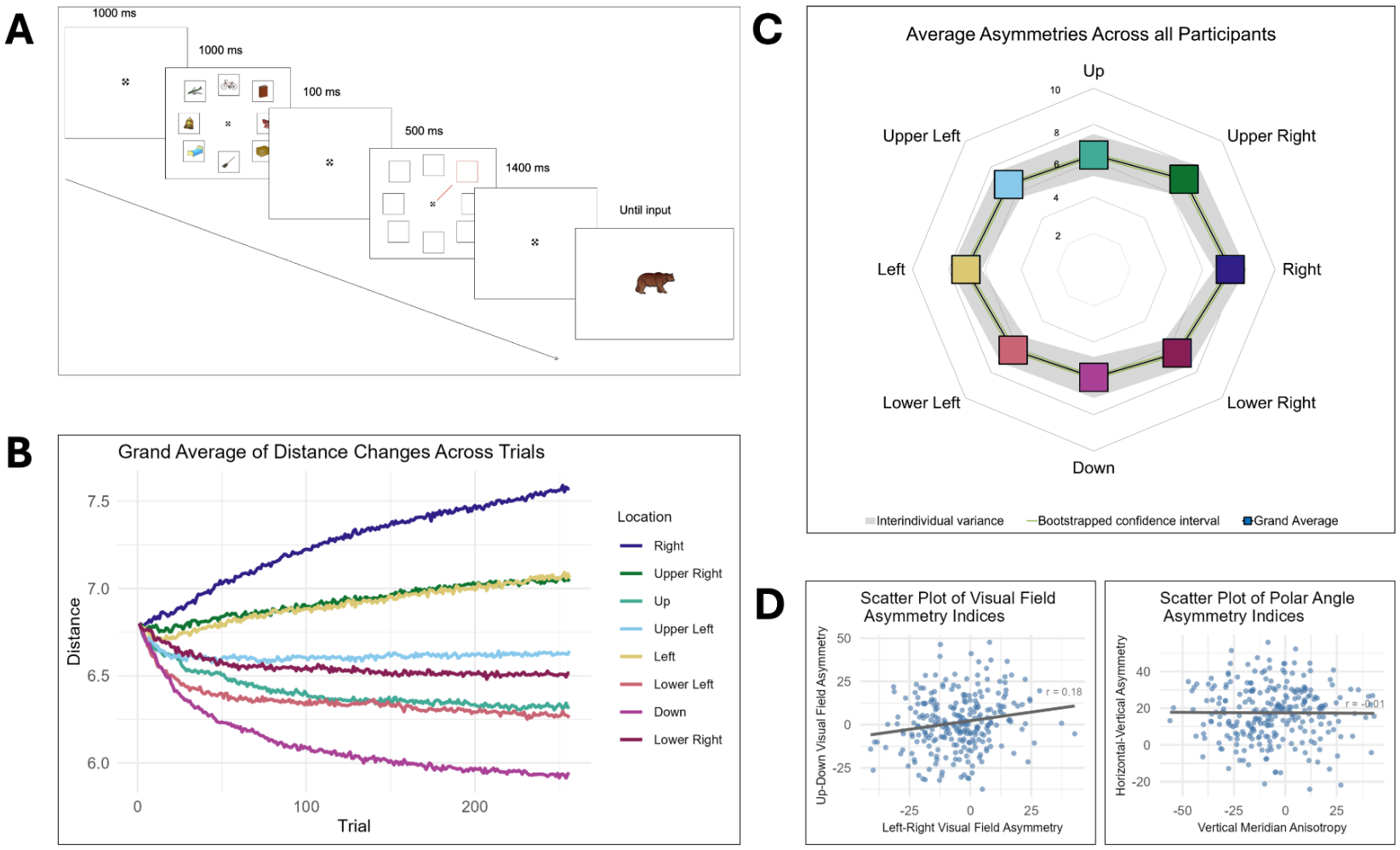
A
1000 ms
1000 ms
100 ms
500 ms
1400 ms
Until input
B
Grand Average of Distance Changes Across Trials
Distance
7.5
7.0
6.5
6.0
0
100
200
Trial
Location
Right
Upper Right
Up
Upper Left
Left
Lower Left
Down
Lower Right
C
Average Asymmetries Across all Participants
Up
Upper Right
Right
Lower Right
Down
Lower Left
Left
Upper Left
10
8
6
4
2
Interindividual variance
Bootstrapped confidence interval
Grand Average
D
Scatter Plot of Visual Field Asymmetry Indices
Up-Down Visual Field Asymmetry
Left-Right Visual Field Asymmetry
r = 0.18
50
25
0
-25
-25
0
25
Scatter Plot of Polar Angle Asymmetry Indices
Horizontal-Vertical Asymmetry
Vertical Meridian Anisotropy
r = -0.01
40
20
0
-20
-50
-25
0
25

Figure 1. **A**: A schematic representation of trial structure. The task included 256 trials, and the locations of the stimuli changed positions on trial by trial basis; **B**: Grand average of distance changes per location across all trials. Note, that distance is described in degrees of polar angle, and that all locations were initially presented at 6.8 degrees from the center of the screen; **C**: Average visual field asymmetries across all participants, calculated based on the mean distances throughout the last 5 trials. The interindividual variance represents mean +/- 1 standard deviation. The bootstrapped confidence interval represents the precision of mean estimates based on the 95% confidence interval of the bootstrapped mean calculated on 1000 resampled datapoints; **D**: Scatter plots represent the relation between different asymmetry indices for individual participants. Please note, that the correlation coefficient of the horizontal-vertical asymmetry and vertical meridian anisotropy correlation is insignificant ($p = 0.9$), consistent with previous studies.

The squares themselves extended 3.3x3.3 degrees of visual angle and were arranged at 0, 45, 90, 135, 180, 225, 270, and 315 degrees of polar angle.

Most importantly, the distance of each square from fixation was continuously and independently adjusted for each of the eight locations throughout the task using the QUEST adaptive staircase procedure (Watson & Pelli, 1983; implemented in PsychoPy, Peirce et al., 2019). Each staircase adaptively targeted the stimulus eccentricity that yielded approximately 63% correct performance above chance, for its specific location, which corresponds to an overall accuracy of 82%. (PsychoPy QuestHandler documentation, and it aligns with performance observed in our prior work (Del Pin et al., 2020). The procedure assumed a standard Weibull psychometric function (50% guess rate, slope ≈ 3.5, lapse rate ≈ 0.01) and used an inverse mapping where the presented distance was calculated as Distance (degrees) = 15 - QUEST_Intensity. This meant that incorrect responses moved stimuli closer to fixation on subsequent trials at that location (decreasing task difficulty), while correct responses moved stimuli further away (increasing difficulty). The operational distance range was 3 to 15 degrees of visual angle, with all locations starting at 6.8 degrees. Consequently, locations where a participant performed better required the stimulus to be placed further away to maintain the target 63% accuracy level, resulting in larger final distances for locations associated with superior performance. Figure 1B depicts the average progression of the distance staircasing for each of the eight locations.

The cued location of each trial, and the target image appearing at that location prior to cueing were determined at the beginning of the experiment. Each location was cued in 32 trials and each of the 200 images appeared at a cued location at least once (whereas a random selection of 56 images appeared twice for a total of 256 trials). The order of the cued locations and the target images at those locations were independently randomized for each participant. On every trial, seven other images were randomly chosen without replacement from the set of all available images (excluding the already designated target image) and assigned to the remaining locations.

Note that despite the heterogeneity of the images with respect to their visual and semantic properties, the fact that the stimulus pool included 200 different images ensures that any single image could not influence the overall asymmetry pattern of the eight target locations in any systematic manner. In other words, even though the images can be expected to vary in their discriminability (as is confirmed by a post-hoc comparison of natural and manmade objects, for example; see SI3A), this should only influence the likelihood of responding correctly or incorrectly on a single trial, but it should not disproportionally bias any one location staircase compared to the other staircases across many consecutive trials. More details regarding the individual images, their average discrimination rates, and comparisons between natural and manmade objects can be found in SI3.

The task was performed in a dimly lit room and presented on an NVIDIA GeForce RTX 2070 SUPER monitor with 60 Hz refresh rate and 1920x1080 screen resolution. The participants were seated approximately 55 cm from the screen and received written instructions for how to perform the task. They were also verbally reminded by the experimenter to always maintain fixation at the center of the screen and not to look at the individual target locations. Responses were given on a standard keyboard with the left and right arrow keys.

Behavioral analysis methods

Because the main outcome of the visual working memory task was the final layout of the eight target locations by the end of the experiment, most participants were included in the analysis. We excluded: trials with reaction times faster than 100 ms from the response screen onset or slower than 3 SD over the individual's mean were removed; all participants who had lower than less than 205 clean trials left (80% of the full experiment) or whose average performance level was lower than 60% correct or who only used one of the response buttons (left/right) in more than 80% of the trials. or who did not finish the experiment on the allotted time. As a result, the analyses were performed on 262 participants (170 F and 92 M, mean age = 23,77; SD = 4,26; 90.45% of the total). Note that for the brain-behavior analyses, 5 additional participants were removed from the dataset because they had poor quality MPM data available from the MRI session (see next section).

The final position of the eight target locations was used to assess the presence of asymmetries in our working memory task. The final position was defined as the average distance of each location over the last five trials of the experiment. This averaging was performed to increase the robustness of the estimates. Other choices, such as averaging the distance of each location over the last five trials where this specific location was cued, led to very similar results (not reported). The distances of the target locations were subsequently aggregated into four summary indices of asymmetries and one summary index of overall vWM performance for each individual participant.

In order to gain a complete overview of the asymmetry effects in our working memory task, both polar angle asymmetries and visual field asymmetries were analyzed. We used the horizontal-vertical asymmetry (HVA) and the vertical meridian anisotropy (VMA) as indices denoting individual polar angle asymmetries. The indices were calculated based on established formulas described by (Himmelberg et al., 2022):

$$HVA = \frac{(mean(left, right) - mean(up, down)}{mean(left, right, up, down)} \times 100$$

$$VMA = \frac{(down - up)}{mean(down, up)} \times 100$$

In addition to the polar angle asymmetries, the broader visual field asymmetries were analyzed to explore the upper versus lower visual field effect, as well as the left versus right visual field effect. To compare the performance in the upper versus lower visual field, the distances of the *upper left, up,* and *upper right* locations were averaged, and compared with analogically computed values for locations *lower left, down,* and *lower right.* A similar approach was used to compare the performance in left vs right visual field, where the distances of the *upper left, left,* and *lower left* locations were averaged and compared with the average distances of the locations *upper right, right,* and *lower right*. The exact formulas for the visual field asymmetry indices were as follows:

$$Upper - Lower\,VFI = \frac{(mean(down, lower\ left, lower\ right) - mean(up, upper\ left, upper\ right))}{mean(down, lower\ left, lower\ right, up, upper\ left, upper\ right,)} \times 100$$

$$Left - Right\,VFI = \frac{(mean(left, upper\ left, lower\ left) - mean(right, lower\ right, upper\ right)}{mean(left, upper\ left, lower\ left, right, lower\ right, upper\ right)} \times 100$$

Note that we specifically chose the visual field asymmetries with inclusion of the locations located on the visual meridians for the main analyses of this study because in a variety of studies the performance in non-meridian locations was notably worse within 30 degrees of visual angle from the center than in on-meridian locations (see: Abrams et al., 2012; Barbot, Xue & Carrasco, 2021; Carrasco et al., 2001; Corbett & Carrasco, 2011), Nevertheless, as can be seen in SI4, the visual field asymmetries calculated with *up, down, left,* and *right* locations removed from the above-described formulas led to very similar results in this sample.

Finally, as a measure of overall visual working memory performance we decided to use the average distance. This index was calculated by simply averaging the final distances across all the eight target locations. Computing such an index for all participants allowed us to test whether the overall working memory performance influenced the asymmetry indices and whether the potential links in the neuroimaging results stem from individual visual working memory performance rather than from perceptual asymmetries. Furthermore, we use this index of overall distance as an approximation of individual vWM performance limits in an attempt to conceptually replicate the findings of Bergmann and colleagues (2016).

The asymmetry indices were analyzed separately and compared to each other, or to other control variables such as eye dominance or participants' height, via paired t-tests, Kruskal-Wallis rank tests, and Pearson correlations. Whenever multiple t-test comparisons were conducted, p-values were adjusted using the Holm–Bonferroni correction. Where applicable, pairs of t-tests were formally compared to determine whether their test statistics and significance levels were systematically different. This was done by performing a paired t-test between the two sets of differences between the data of interest (Nieuwenhuis et al., 2011). Similarly, pairs of correlations were formally compared using a bootstrap resampling approach and implemented with the *boot* package in R (Canty & Ripley,

2022; Davison & Hinkley, 1997). 999 bootstrap samples were used to recalculate the correlation coefficient pairs, and eventually the differences between them. Finally, a 95% confidence interval was derived for the observed differences.

All statistical analyses for the behavioral data were performed using R version 4.3.1 (2023-06-16 ucrt; R Core Team, 2023) and various packages, including *tidyverse* (Wickham et al., 2019), *effsize* (Torchiano & others, 2020), and *reshape* (Wickham, 2007).

MRI acquisition

The MRI data was acquired at a Siemens Magnetom Skyra 3T MR scanner. Each participant underwent resting-state fMRI, quantitative multi-parameter mapping (MPM), and diffusion-weighted imaging in one scanning session lasting approximately one hour. This study uses only the MPM data. MPM allows for the acquisition of quantitative MRI (Weiskopf et al., 2013), with each contrast being sensitive to different microstructural aspects of the neural tissue: magnetization transfer (MT) reflecting the myelination (Bjarnason et al., 2005), effective proton density (PD) corresponding to the water content (Lorio et al., 2019), longitudinal relaxation rate (R1) corresponding to the water mobility in its microenvironment and iron content of the neural tissue (Callaghan et al., 2015), and effective transverse relaxation rate (R2*) representing the iron accumulation in the tissue (Draganski et al., 2011).

The MPM protocol was implemented based on the recommended Siemens vendor sequence (Leutritz et al., 2020). Three-dimensional data acquisition consisted of three multi-echo spoiled gradient echo scans (i.e., fast low angle shot [FLASH] sequences with magnetization transfer saturation (MT), T1, and effective proton density (PD) contrast weighting). Additional reference radio-frequency (RF) scans were acquired. The acquisition protocol had the following parameters: TR of PDw and T1w contrasts: 18 ms; TR of MTw contrast: 37 ms; minimum/maximum TE of PDw, T1w and MTw contrasts: 2.46/14.76 ms; flip angles for MTw, PDw and T1w contrasts: 6°, 4°, 25°, respectively; six equidistant echoes; 1 mm isotropic reconstruction voxel size; Field of view 224 ´ 256 ´ 176 mm; AP phase encoding direction; GRAPPA parallel imaging speedup factor of 2; T1w, PDw and MTw acquisition times: 3:50, 3.50, 7.52. The acquisition of low-resolution three-dimensional spoiled gradient echo volumes was executed using both the RF head coil and the body coil. This dual acquisition facilitated the generation of a relative net RF receive field sensitivity (B1−) map for the head coil. The approach obtained rapid acquisition by maintaining a low isotropic spatial resolution of 4^3 mm3, a short echo time (TE) of approximately 2 ms, and a reduced flip angle of 6°, avoiding parallel imaging acceleration or partial Fourier. This procedure of capturing volume pairs with the

head and body coils was systematically repeated before acquiring each of the MT, PD, and T1 contrasts.

MRI preprocessing

The raw MPM data was converted into the four maps (MT, PD, R1, P2*) via the standard recommended map creation module provided by the hMRI-toolbox, a dedicated SPM add-on for MPM data analysis (Tabelow et al., 2019). The map creation includes an auto-reorientation step and two steps for correcting the quantitative MRI estimates for spatial receive and transmit field inhomogeneities, respectively. At this stage, all resulting maps were also visually inspected, and participants with strong movement artifacts or abnormal brain anatomy (i.e., large ventricles or visible tumors) were excluded from further analysis, leading to exclusion of 5 additional participants (resulting in a total of 257 participants left for the MRI analysis). Further preprocessing steps followed the voxel-based quantification (VBQ) pipeline, which is very similar to the typical voxel-based morphometry (VBM) pipeline for volumetric structural analysis in SPM. The pipeline was performed on the individual MT maps first, and the transformations were subsequently applied to the other maps as well. In short, the VBQ pipeline first segments each image into gray matter, white matter, and cerebrospinal fluid. Next, all individual images are spatially registered to a group average with the DARTEL algorithm. Finally, each tissue type is smoothed with a 4 mm FWHM kernel. Note that the final step deviates slightly from the standard VBM pipeline. For MPM data, a specialized tissue weighted smoothing algorithm is performed in order to avoid partial volume effects at tissue boundaries and distort the quantitative estimates.

In order to perform surface-based structural analyses in addition to the volumetric analysis described above, a synthetic T1w image was generated from the R1 and PD maps. First, both maps were thresholded to achieve the required FreeSurfer units (Fischl et al., 1999). The R1 map was divided by itself two times, thresholded at zero, and multiplied by one thousand. The PD map was thresholded by zero and multiplied by one hundred. All manipulations were performed using FSL maths commands. Subsequently, the mri_synthesize FreeSurfer command was applied to create a synthetic FLASH image based on the T1 and PD maps. The optional flagged argument for optimal gray and white matter contrast weighting was used with the parameters 20, 30, and 2.5. Finally, the synthetic T1w image was divided by four to comply with the scale that FreeSurfer expects.

The surface reconstructions for estimating cortical thickness were created with the standard pipeline of the CAT12 toolbox (Gaser et al., 2024). The pipeline uses a projection-based thickness method (Dahnke et al., 2013) and surface refinement to create a model of the cortical sheet and folding patterns. Topological defects are automatically repaired using spherical harmonics and individual

central surfaces are spatially registered via spherical mapping with minimal distortions. Finally, local thickness values are transferred to the Freesurfer 'fsaverage' template.

MRI analysis

Statistical analyses were conducted for both the volumetric MPM data and the surface-based cortical thickness data. As for MRI preprocessing, VBQ was performed with the SPM12 toolbox (Wellcome Trust Centre for Neuroimaging, 2014), and the cortical thickness analysis was performed on the synthetic T1 maps with the CAT12 toolbox (Gaser et al., 2024).

ROI analysis

For VBQ, the region of interest (ROI) analysis focused on the primary visual cortex V1 to investigate the sensory recruitment hypothesis. In addition to V1, we tested two non-sensory control regions known for their role in the processing of visual working memory. These additional regions of interest were the intraparietal sulci (IPS; Bettencourt & Xu, 2016; Iamshchinina et al., 2021), and the frontal eye fields (FEF; Jerde et al., 2012; Lefco et al., 2020; Offen et al., 2010). Importantly, FEF include the superior precentral sulcus (sPCS; Bedini et al., 2023), an area linked with the maintenance of the visual working memory representations (Jerde et al., 2012).

The analysis was performed using atlas-based masks created with the WFU Pick Atlas toolbox (Maldjian et al., 2003). The individual 3D masks covered Brodmann area 17, which covers V1 bilaterally, and Brodmann area 6, which covers the frontal eye fields bilaterally. Additional masks of the early visual cortex were created for control analysis to check how systematic any V1-related results were. The chosen areas included left BA 17, right BA 17, BA 18 (which covers V2 bilaterally), and BA 17+18. All masks created with the WFU Pick Atlas toolbox were created with the dilation of 1. Spherical masks of intraparietal sulci were created with the Marsbar toolbox (Brett et al., 2002) based on the coordinates described in the literature (see: Gayet et al., 2017; Knops et al., 2006; Lu et al., 2016; Schneiders et al., 2011). The MNI coordinates were 38, -42, 44 for right IPS and -40, -42, 46 for left IPS, and the spheres had the radius of 10.

For all indices, the analysis was performed as follows. All voxels within the chosen ROI were averaged for each participant. Then, two mixed-effect linear models were fitted and compared using a likelihood ratio test. One model included total intracranial volume, age, and sex as nuisance covariates, and the participant as a random effect, supporting the null hypothesis. The second one comprised the asymmetry index as a predictor, the same nuisance covariates, and the participant as a random effect, supporting the alternative hypothesis. This analysis was performed for each of the four MPM contrasts (MT, PD, R1, and R2*), each of the ROIs, and each of the behavioral indices

separately. Finally, the results were corrected for multiple comparisons within each index using the False Discovery Rate (FDR) method to control for the expected proportion of false positive results.

The ROIs for the cortical thickness analysis were derived from the Human Connectome Project multimodal parcellation atlas (Glasser et al., 2016). The regions of interest were analogical to the ones picked for VBQ and included the early visual cortex (V1), intraparietal sulci (IPS1), and the frontal eye field (FEF). The statistical procedure was very similar to VBQ. I.e., the basic model included age and sex as nuisance covariates, the behavioral index as a predictor and cortical thickness as the predicted variable. A separate model was built for each of the five behavioral indices of interest and its relation to cortical thickness was assessed via a drop-one contrast.

Whole brain analysis

Previously-estimated gray matter models were used for the whole-brain statistical analysis. The data was analyzed separately for the HVA and the VMA indices, as well as for the upper-lower and left-right visual field indices, and finally the average distance of all target locations. Likelihood ratio tests were performed, comparing models including the behavioral index, sex, age, and total intracranial volume as predictors, and the voxel volume as the predicted variable against models without the behavioral indices. If the behavioral indices would significantly impact the brain structure, voxel clusters would be found as a result of the analysis. The Holm-Bonferroni correction method was used for whole-brain analysis to control for the family-wise error rate.

Results

Behavioral results

The behavioral task in this study was designed to map out inhomogeneities in working memory performance across the visual field. We summarized the spatial inhomogeneities via polar angle and visual field asymmetry indices and tested whether these distributions of indices differed reliably from zero. The horizontal-vertical asymmetry (HVA) reached an average value of 17.5 (min = -24.14, max = 55.88, SD = 14.7) and the distribution differed significantly from zero ($t(261) = 19.26$, $p < 0.001$, Cohen's d = 1.19). This indicates that on average, participants' performance was better along the horizontal axis compared to the vertical axis, as expected. The vertical meridian anisotropy (VMA) reached an average of -6.15 (min = -56.02, max = 43.18, SD = 19.64), and this distribution too differed significantly from zero ($t(261)= -5.07$, $p < 0.001$, Cohen's d = -0.31).

As for the visual field asymmetries, the left-right asymmetry reached and average value of -4.83 (min = -40.93, max = 42.86, SD =13.98) and the distribution differed significantly from zero (t(261)=

-5.59, $p < 0.001$, Cohen's $d = -0.35$). The superior performance in the right visual field was not related to the eye-dominance of the participants ($\chi 2 = 0.07$, $p = 0.94$). The upper-lower asymmetry reached an average value of -11.43 (min = -51.72, max = 23.16, SD = 15.29) and its distribution differed significantly from zero as well ($t(261) = -12.1$, $p<0.001$, Cohen's $d = -0.75$). Similar to VMA, the polarity of the upper-lower asymmetry indicates better performance in the upper compared to the lower visual hemifield, on average. This similarity was further supported by a significant correlation between the two indices ($r(260)=0.58$, $p<0.001$).

To summarize, the results demonstrate clear spatial inhomogeneities in a visual working memory task both along the polar angles and across the visual field. We next turn to the question of whether the interindividual differences within the polar angle asymmetries or between-visual field asymmetries are related to each other. A Pearson's correlation test between the VMA and HVA yielded a clear null result ($r(260) = -0.01$, $p = 0.9$, 95% CI [–0.13, 0.11]). The upper-lower and left-right asymmetries, on the other hand, were weakly yet significantly correlated ($r(260) = 0.25$, $p<0.01$, 95% CI [0.13, 0.36]). A test between the strength of these two correlations also confirmed that the latter is systematically stronger than the former (95% bootstrap confidence interval ranging from -0.39 to -0.1) indicating that visual field asymmetries share a source of variance whereas polar angle asymmetries do not (the same has been reported previously by Himmelberg et al., 2020 and 2022, and Barbot et al., 2021).

The above-described pattern of results mostly confirmed our a priori expectations, including the inverted VMA direction. In an effort to eliminate potential confounding sources for this finding, we tested whether the interindividual variability in VMA could potentially be linked to the height of the participants (as the viewing angle of the computer screen certainly differed to some extent between tall and short participants). This correlation was not significant ($r(260) = -0.02$, $p=0.79$). The variability of VMA was also not related to the eye-dominance of the participants ($\chi 2 = 1.04$, $p = 0.31$). See SI3 for correlations of height and eye-dominance with the other asymmetry indices. We therefore conclude that, contrary to many other visual tasks, performance in our visual working memory task is better along the upper vertical meridian compared to the lower vertical meridian.

Finally, we also assessed the average distance of the eight target locations at the end of the task. As the staircase was used to adjust the distance of the locations from the center of the screen, the final average distance was highly correlated with accuracy ($r = 0.86$, $p < 0.001$). Because of that, we decided to use the average distance as a measure of overall visual working memory performance in our study. The average distance from the center of the screen varied between 5.39 and 8.08 visual angle degrees (mean = 6.67, SD = 0.52). Note that polar angle asymmetry patterns were not confounded by average distance, with the VMA not being significantly correlated with the average distance ($r = -0.01$, $p = 0.83$) and HVA manifesting a negligible correlation with the average distance ($r = 0.14$, $p = 0.03$). Contrarily, visual field asymmetry was moderately correlated ($r = 0.45$, $p < 0.001$ for the up-down asymmetry and $r = 0.48$, $p <0.001$ for the left-right asymmetry). This effect was expected, as the visual field asymmetries rely on the average distances in the hemifields. Additionally, we assessed whether the participants' average reaction time is linked with the accuracy of the task performance or with the average distance of the locations from the center of the screen by the end of the task. The correlations were negligible and were not statistically significant. For details see SI5.

Brain-behavior relationships

The behavioral results confirm that there are systematic inhomogeneities in the visual working memory performance across the visual field. These inhomogeneities were reliable for the polar angle indices as well as for the visual field indices. We next investigate whether these behavioral patterns can be linked to interindividual differences in brain structure.

Given that the hypotheses of this work are specifically targeted at the early visual cortex and its potential links to working memory performance, we focus mainly on ROI analysis of V1 (and V2 in SI), with IPS and FEF as control regions. The latter two regions have been consistently linked to vWM performance, but they do not afford detailed perceptual representations of the memory content. Therefore, if interindividual differences in behavior would be linked to structural differences in IPS/FEF but not V1, our data would speak against the sensory recruitment hypothesis. If, on the other hand, the behavioral patterns would be linked to V1 structure (regardless of IPS/FEF results) we would interpret this as supporting the sensory recruitment hypothesis. Whole-brain analyses will be presented for completeness as well.

In the following, we will first analyze volumetric differences in the four MPM maps, where each map is informative about different microstructural tissue properties. Second, interindividual differences in cortical thickness – derived from the synthetic T1w structural image – will be related to the behavioral results.

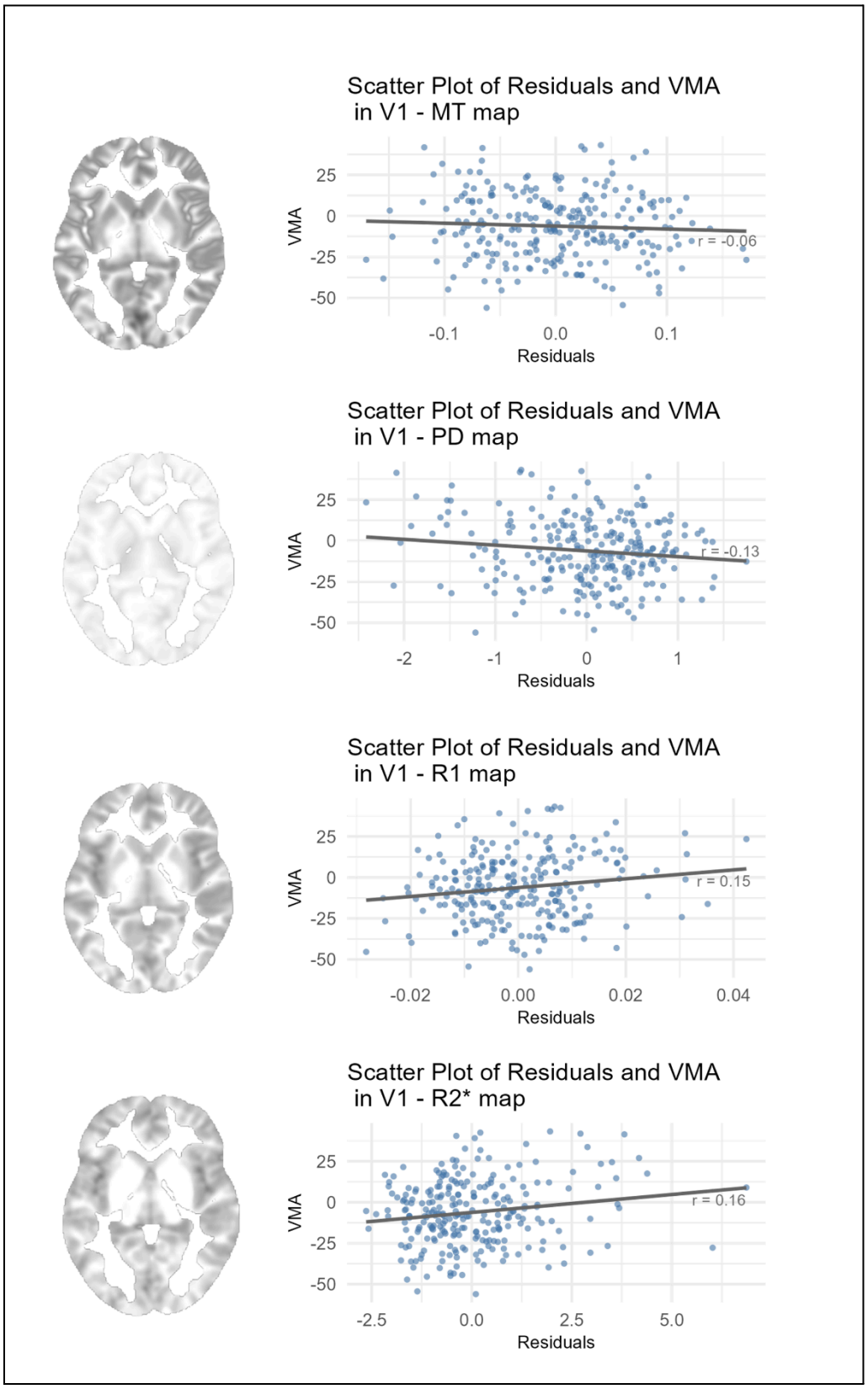

Figure 2. Scatter plots of VMA index values and residuals of the mixed-effect linear model including averaged V1 volume as a predicted value, along with sex, age and total intracranial volume as predictors and participant as a random effect for MT, PD, R1 and R2* multiparametric maps. Each data point corresponds to a participant.

Volumetric results

A set of regression analyses relating the behavioral asymmetry indices to the four different MPM maps across the three ROIs delivered mostly null results (For details see Table 1). Three MPM parameters – R2*, PD, and R1 in V1 – showed significant associations with the behavioral VMA index. For example, the R2* map is primarily indicative of the iron content in brain tissue, and PD and R1 maps are linked with the total water content and a combination of molecular water mobility and iron content of the tissue respectively. This means that participants with a more pronounced behavioral VMA index tended to have a more dense structure of neural tissue in V1, with lower water content and higher iron concentration compared to participants with less asymmetry along the vertical meridian (see: Figure 2). Additional analyses revealed that this link between PD, R1, and R2* and the behavioral VMA index was only robust with the left V1 and not right V1, and that the results were not consistent for V2 or V1+V2 combination (see: SI6). The same set of analyses for the upper-lower visual field asymmetry did not reach significance. Moreover, no significant effects were found in FEF or IPS gray matter for any of the behavioral asymmetry indices. Nevertheless, direct comparisons between the PD, R1, and R2* correlation strengths revealed that the VMA effects were not significantly stronger than the effects with the next highest $\chi 2$ value within the same MPM maps (95% bootstrap confidence interval ranging from -0.1855 to 0.1294 for PD, from -0.1514 to 0.2278 for R1, -0.0719 to 0.2345 for R2*). This indicates that despite the significance of the PD, R1, and R2* results, the current analysis may be lacking in power to uncover smaller effects present in the data.

In addition to the behavioral asymmetry indices, identical analyses were performed for the average distance to assess whether there are any structural correlates of the overall visual working memory performance. The purpose of these analyses was to conceptually replicate the findings of Bergmann and colleagues (2016), who reported a link between V1 gray matter volume and individual performance limits in a vWM task. None of the regression models, including average distance as a predictor, were significant in our dataset, however.

We also conducted a whole-brain analysis, searching for clusters of voxels whose volume would explain more variance in the behavioral asymmetries. No such clusters were found for any of the asymmetry indices in any of the MPM maps.

	Bilateral V1 multiparametrical maps								**V1 cortical thickness**			
	MT		**PD**		**R1**		**R2***		**Left V1**		**Right V1**	
Index	χ2(1)	p	χ2(1)	p	χ2(1)	p	χ2(1)	p	F	p	F	p
Horizontal-Vertical Asymmetry	0.45	0.729	0.39	0.729	0.12	0.729	0.13	0.729	1.06	0.305	0.244	0.622
Vertical Meridian Anisotropy	0.85	0.36	**4.4**	**0.048**	**6.08**	**0.027**	**6.76**	**0.027**	0.61	0.435	1.6	0.207
Upper-Lower Visual Field Index	1.95	0.172	1.86	0.172	1.97	0.172	0.71	0.172	0.61	0.435	0.45	0.504
Left-Right Visual Field Index	0.2	0.65	1.69	0.39	3.4	0.26	0.9	0.46	0.8	0.373	0.01	0.933
Average Distance	0.93	0.867	<0.001	0.984	0.04	0.984	0.64	0.867	0.29	0.589	0.1	0.754
	Bilateral IPS multiparametrical maps								**IPS cortical thickness**			
	MT		**PD**		**R1**		**R2***		**Left IPS**		**Right IPS**	
Index	χ2(1)	p	χ2(1)	p	χ2(1)	p	χ2(1)	p	F	p	F	p
Horizontal-Vertical Asymmetry	0.05	0.82	0.51	0.82	1.29	0.82	0.21	0.82	0.18	0.676	2.56	0.111
Vertical Meridian Anisotropy	0.004	0.95	0.09	0.95	0.61	0.87	0.68	0.87	0.69	0.406	1.36	0.245
Upper-Lower Visual Field Index	0.28	0.802	0.22	0.802	0.06	0.802	0.79	0.802	0.001	0.970	1.74	0.188
Left-Right Visual Field Index	3.94	0.19	0.85	0.85	0.71	0.4	0.27	0.61	0.93	0.335	0.19	0.661
Average Distance	2.68	0.388	0.13	0.72	1.69	0.388	0.25	0.72	2.35	0.127	2.97	0.08
	Bilateral FEF multiparametrical maps								**FEF cortical thickness**			
	MT		**PD**		**R1**		**R2***		**Left FEF**		**Right FEF**	
Index	χ2(1)	p	χ2(1)	p	χ2(1)	p	χ2(1)	p	F	p	F	p
Horizontal-Vertical Asymmetry	<0.001	0.997	1.07	0.603	0.009	0.997	1.2	0.603	0.47	0.495	0.51	0.475
Vertical Meridian Anisotropy	0.92	0.777	0.08	0.777	1.24	0.531	1.33	0.531	0.16	0.686	2.66	0.104
Upper-Lower Visual Field Index	0.92	0.45	2.49	0.45	0.15	0.695	1.35	0.45	0.55	0.458	2.55	0.111

Left-Right Visual Field Index	0.2	0.707	0.14	0.707	0.34	0.707	0.19	0.707	0.16	0.688	0.2	0.656
Average Distance	0.13	0.746	0.34	0.746	1.3	0.746	0.11	0.746	0.83	0.362	0.21	0.646

Table 1. Volumetric and cortical thickness results. The results of the Likelihood Ratio tests are comparing more complex models (df = 7) explaining the variance of the ROI voxels against simpler ones (df = 6). The p values were corrected for comparisons of different maps within each index using the FDR correction. The cortical thickness results displays the F statistics and uncorrected p values for different indices and regions of interest.

Cortical thickness results

Cortical thickness was analyzed very similarly to the volumetric MPM data, i.e., average cortical thickness of the three ROIs was regressed on the behavioral indices and nuisance variables. None of the asymmetry indices nor the average distance constituted significant predictors in these models (for details see Table 1). In an exploratory whole-brain analysis (implemented in CAT12), we tested cortical thickness across all atlas-defined regions with a Holm-Bonferroni correction for multiple comparisons. This analysis revealed significant correlations between the left-right visual field asymmetry and cortical thickness in two regions: the left V3 ($F = 9.87$, $p = 0.041$) and right Brodmann's area 25 (subgenual area; $F = 4.45$, $p = 0.036$). Due to those findings, we performed an additional post-hoc examination of the V3 and BA 25 ROI results for other indices. Among the mainly null results there was a significant V3 result for the average distance ($F = 8.81$, $p = 0.003$). The whole-brain analysis had no statistically significant results for the other visual field indices.

Discussion

This study examined whether structural properties of the early visual cortex explain asymmetries in visual working memory (vWM) performance. Behavioral results of the vWM task are consistent with the well-established perceptual asymmetries, including a strong horizontal–vertical asymmetry (Montaser-Kouhsari & Carrasco, 2009), a left–right asymmetry favoring the right hemifield (Karim & Kojima, 2010) and an inverted vertical meridian anisotropy, with better performance in the upper than the lower vertical meridian of the visual field, consistent with Del Pin et al. (2020), but contrary to the findings of Montaser-Kouhsari & Carrasco, (2009).Individual asymmetry indices were then tested as predictors of cortical structure. While no effects emerged in IPS or FEF, V1 architecture was linked to VMA across PD, R1, and R2* maps.

Importantly, we also identified a connection between the cortical thickness of the left V3 and both the left-right visual asymmetry and the average distance index. As task performance was generally better for stimuli presented in the right, upper right, and lower right locations, the association within the left visual cortex, which is responsible for processing the right visual field (Sereno et al., 1995), is anatomically meaningful. V3 has previously been linked with conscious perception and stimulus discrimination (Salminen-Vaparanta et al., 2019), which could account for the enhanced performance in the right hemifield among participants with a thicker V3. Additionally, we observed a relationship between left-right asymmetry and the thickness of the right subgenual area (BA 25). Since this brain region is primarily involved in emotional regulation (Mayberg et al., 1999) and autonomic functions (Sudheimer et al., 2015; Wallis et al., 2017), we consider this finding to be incidental.

The behavioral results of our study yielded several noteworthy visual asymmetry patterns. First, we found that the performance in the right visual hemifield was better than in the left hemifield, which was unanticipated. Numerous previous studies examining asymmetrical patterns in visual working memory or visuospatial working memory tasks did not exhibit this kind of effect, as due to the bilateral field advantage, both hemispheres should have separate attentional resources (Strong & Alvarez, 2020; Zhang et al., 2017), allowing for unified performance across the hemifields. However, there is previous evidence of the right visual hemifield manifesting improved performance in cognitive tasks (Karim & Kojima, 2010). Another potential explanation of such an effect could be the content of the stimuli, some of which included tools among other manmade or natural objects. As described by Garcea et al., (2012), tools are generally better recognized in the right visual field due to the overrepresentation of tool-related knowledge in the left hemisphere. Despite that, in our study, the type of objects used in the tasks (natural or manmade, including tools) did not affect the performance at any of the locations (see: SI2)

Moreover, the upper-lower visual field asymmetries were found to be inverted to previous literature, which describes the lower visual field dominance in various perceptual and cognitive tasks, both regarding the whole lower hemifield (Karim & Kojima, 2010) and its fragment within 30 visual angle degrees to the vertical meridian (see: Abrams et al., 2012; Carrasco et al., 2001; Corbett & Carrasco, 2011). Albeit, the previous data is inconsistent, with some studies suggesting, that humans should typically recognize objects with higher accuracy in the upper than in the lower visual field (Chambers et al., 1996; Del Pin et al., 2020; Zito et al., 2016), while other studies exploring if the perceptual asymmetries carry over to working memory tasks proved increased working memory performance in the lower visual hemifield (Genzano et al., 2001), particularly the lower vertical meridian (Montaser-Kouhsari & Carrasco, 2009). At the present state of knowledge, it is difficult to conclusively interpret the inverted VMA polarity in our results. Further studies are needed to explore the potential origins of this effect.

The average distance from the center of the screen was used as a marker of overall visual working memory performance. It was found to be moderately correlated with the upper-lower and left-right hemifield asymmetries, but its link with the HVA was negligible, and with VMA – non-significant. This finding could point out the unique properties of VMA, which is represented cortically at the verge of the right and left hemispheres (Glickstein & Whitteridge, 1987).

The horizontal-vertical asymmetry, which was the most pronounced asymmetry pattern in the performance of our object recognition task, was not significantly linked to V1 structure in any of the multiparametric maps. In contrast, the comparatively small and inverted vertical meridian anisotropy was proved to be linked with the individual differences in V1 structure. This finding goes against the

existing literature, which links both HVA and VMA with both the structure and function of the early visual cortex (Himmelberg et al., 2023). Nevertheless, as the HVA and VMA are known to be uncorrelated (Barbot et al., 2021; Himmelberg et al., 2020, 2022; Purokayastha et al., 2021), our findings may point towards the conclusion, that they could arise from distinct neural underpinnings, in agreement with such a suggestion in the aforementioned studies. This interpretation would tie in with the finding of individual polar angle asymmetries being at least partially heritable (Benson et al., 2021).

We found the vertical meridian anisotropy to be linked with three MPM maps: PD, R1 and R2*. PD contrast reflects the free water content in the neural tissue (Lorio et al., 2019) whereas R1 reflects water fluctuations in the tissue microenvironments and iron content of the neural tissue (Callaghan et al., 2015). Interestingly, the R2* map is known to reflect the iron accumulation in the neural tissue (Draganski et al., 2011). Previous research linked the increased iron accumulation in brain tissue with factors such as high body mass index and diet (Pirpamer et al., 2016), age, or smoking (Hagemeier et al., 2015). Moreover, it has also been linked with impairment of memory and general cognitive functions in adults (Spence et al., 2020), including those accompanying neurodegeneration in Alzheimer's disease (Raven et al., 2013) as well as with the stable trait of intelligence (Pirpamer et al., 2016). Similarly, R1 was proven to be linked with impaired cognitive performance in patients with mild cognitive impairment (Granziera et al., 2015). Yet, none of the aforementioned studies aimed at assessing iron accumulation specifically in the early visual cortex. Wenger and colleagues (2022) point out, that while MT and PD maps manifest high reliability, the reliability of R1 and R2* maps is limited in healthy young adults, with the intraclass correlation coefficient (ICC) being reported as high for MT (0.88) and PD (0.87), and moderate for R1 (0.73) and R2* (0.78). This phenomenon could be linked to the generally low variability of iron deposition and molecular mobility of water in the neural tissue in this group. Nevertheless, their study consisted of a substantially smaller sample (15 participants) and did not include the early visual cortex as a region of interest for the reliability examination. Future studies on a broader age range of participants are needed to establish whether the increased iron accumulation in V1 impacts the decreased asymmetries in visual working memory performance.

Our findings regarding the V1 surface differences are in partial agreement with the findings of Bergmann and colleagues (2016): we found a link between the working memory performance and the structure of V1. Importantly, our findings had a rather small effect and only applied to certain MPM maps with only one out of four asymmetries of vWM performance whereas in the Bergmann study, the overall vWM performance was tested against T1 weighted MRI scans, with V1 identified with the use of retinotopic mapping, allowing for more precision compared with the atlas-based ROI choice in our

study. Moreover, we did not confirm their finding regarding the V1 cortical thickness link to the vWM performance, but we did find a link between vWM performance and V3 cortical thickness which corroborates the role of early visual cortex in working memory related brain functions.

Despite promising results, our study has several limitations. Firstly, the study would benefit from using a chinrest while performing the behavioral task. This would improve the data stability and further minimize the risk of participants altering their distance from the screen. As the fixation and eye movements had not been controlled for with any eye-tracking device and the stimuli were presented for 1000 ms each, there exists a possibility of the dataset being confounded by scanning bias (Carrasco et al., 1995; Rezec & Dobkins, 2004). Albeit, the stimuli were presented in random locations and the fixation cross used in the study had been designed specifically to improve fixation (Thaler et al., 2013). To exclude the possibility of the viewing angle or eye dominance impacting the asymmetry patterns found in the performance of our task, we performed a post-hoc analysis, examining the effect of height on individual asymmetry indices, yet we did not obtain any significant results (see: SI3). Finally, our study did not include the individual retinotopic mapping, which would have improved the accuracy of V1 selection compared to the atlas-based approach and would have allowed for more detailed structural analysis within V1.

Funding

This work was supported by the National Science Centre in Poland (Grant nr. 2021/42/E/HS6/00425). The data collection was conducted as part of the COST Action *The Neural Architecture of Consciousness*, CA18106, (European Cooperation in Science and Technology) and supported by the National Science Centre grant nr. 2017/27/B/HS6/00937. JPK was additionally supported by the National Science Centre grant nr. 2024/53/N/HS6/04123. Centre for Brain Research is supported as a flagship project by Future Society Priority Research Area and Quality of Life Priority Research Area under the Strategic Program of Excellence Initiative at the Jagiellonian University.

Acknowledgements

We thank the entire NeuralArchCon consortium (www.neuralarchcon.org). We thank Katarzyna Hat and Monika Ostrogorska for collecting the MRI data. We thank Tomasz Kostka, Wiktoria Orłowska, and the C-lab interns between 2020-2022 for their assistance in the behavioral data collection.

References

Abrams, J., Nizam, A., & Carrasco, M. (2012). Isoeccentric locations are not equivalent: The extent of the vertical meridian asymmetry. *Vision Research*, *52*(1), 70–78. https://doi.org/10.1016/j.visres.2011.10.016

Adam, K. C., Rademaker, R. L., & Serences, J. T. (2022). Evidence for, and challenges to, sensory recruitment models of visual working memory. *Visual Memory*, 5–25.

Barbot, A., Xue, S., & Carrasco, M. (2021). Asymmetries in visual acuity around the visual field. *Journal of Vision*, *21*(1), 2. https://doi.org/10.1167/jov.21.1.2

Bedini, M., Olivetti, E., Avesani, P., & Baldauf, D. (2023). Accurate localization and coactivation profiles of the frontal eye field and inferior frontal junction: An ALE and MACM fMRI meta-analysis. *Brain Structure and Function*, *228*(3–4), 997–1017. https://doi.org/10.1007/s00429-023-02641-y

Benson, N. C., Kupers, E. R., Barbot, A., Carrasco, M., & Winawer, J. (2021). Cortical magnification in human visual cortex parallels task performance around the visual field. *eLife*, *10*, e67685. https://doi.org/10.7554/eLife.67685

Bergmann, J., Genç, E., Kohler, A., Singer, W., & Pearson, J. (2016). Neural Anatomy of Primary Visual Cortex Limits Visual Working Memory. *Cerebral Cortex*, *26*(1), 43–50. https://doi.org/10.1093/cercor/bhu168

Bettencourt, K. C., & Xu, Y. (2016). Decoding the content of visual short-term memory under distraction in occipital and parietal areas. *Nature Neuroscience*, *19*(1), 150–157. https://doi.org/10.1038/nn.4174

Bjarnason, T., Vavasour, I., Chia, C., & MacKay, A. (2005). Characterization of the NMR behavior of white matter in bovine brain. *Magnetic Resonance in Medicine: An Official Journal of the International Society for Magnetic Resonance in Medicine*, *54*(5), 1072–1081.

Brett, M., Anton, J.-L., Valabregue, R., Poline, J.-B., & others. (2002). Region of interest analysis using an SPM toolbox. *8th International Conference on Functional Mapping of the Human Brain*, *16*(2), 497.

Callaghan, M. F., Helms, G., Lutti, A., Mohammadi, S., & Weiskopf, N. (2015). A general linear relaxometry model of R_1 using imaging data: General Linear Relaxometry Model of R1. *Magnetic Resonance in Medicine*, *73*(3), 1309–1314. https://doi.org/10.1002/mrm.25210

Canty, A., & Ripley, B. D. (2022). *boot: Bootstrap R (S-Plus) Functions*.

Carrasco, M., Evert, D. L., Chang, I., & Katz, S. M. (1995). The eccentricity effect: Target eccentricity affects performance on conjunction searches. *Perception & psychophysics*, *57*(8), 1241-1261.

Carrasco, M., P.Talgar, C., & Cameron, E. L. (2001). Characterizing visual performance fields: Effects of transient covert attention, spatial frequency, eccentricity, task and set size. *Spatial Vision*, *15*(1), 61–75. https://doi.org/10.1163/15685680152692015

Chambers, K., McBeath, M., Schiano, D., & Metz, E. (1996). Viewers preferentially attend to the tops of figures. *Investigative Ophthalmology and Visual Science*, *37*(3), S178.

Christophel, T. B., Klink, P. C., Spitzer, B., Roelfsema, P. R., & Haynes, J.-D. (2017). The distributed nature of working memory. *Trends in Cognitive Sciences*, *21*(2), 111–124.

COST (European Cooperation in Science and Technology). (2018). *Technical Annex of Action CA18106: The neural architecture of consciousness* [Memorandum of Understanding]. https://e-services.cost.eu/files/domain_files/CA/Action_CA18106/mou/CA18106-e.pdf

Corbett, J. E., & Carrasco, M. (2011). Visual Performance Fields: Frames of Reference. *PLoS ONE*, *6*(9), e24470. https://doi.org/10.1371/journal.pone.0024470

Cowan, N. (2017). The many faces of working memory and short-term storage. *Psychonomic Bulletin & Review*, *24*, 1158–1170.

Cronbach, L. J. (1957). The two disciplines of scientific psychology. *American Psychologist*, *12*(11), 671.

Curcio, C. A., & Allen, K. A. (1990). Topography of ganglion cells in human retina. *Journal of Comparative Neurology*, *300*(1), 5–25.

Curcio, C. A., Sloan, K. R., Kalina, R. E., & Hendrickson, A. E. (1990). Human photoreceptor topography. *Journal of Comparative Neurology*, *292*(4), 497–523.

Davison, A. C., & Hinkley, D. V. (1997). *Bootstrap Methods and Their Applications*. Cambridge University Press. http://statwww.epfl.ch/davison/BMA/

Del Pin, S. H., Skóra, Z., Sandberg, K., Overgaard, M., & Wierzchoń, M. (2020). Comparing theories of consciousness: Object position, not probe modality, reliably influences experience and

accuracy in object recognition tasks. *Consciousness and Cognition*, *84*, 102990. https://doi.org/10.1016/j.concog.2020.102990

Dimond, D., Perry, R., Iaria, G., & Bray, S. (2019). Visuospatial short-term memory and dorsal visual gray matter volume. *Cortex*, *113*, 184-190. https://doi.org/10.1016/j.cortex.2018.12.007

Draganski, B., Ashburner, J., Hutton, C., Kherif, F., Frackowiak, R. S. J., Helms, G., & Weiskopf, N. (2011). Regional specificity of MRI contrast parameter changes in normal ageing revealed by voxel-based quantification (VBQ). *NeuroImage*, *55*(4), 1423–1434. https://doi.org/10.1016/j.neuroimage.2011.01.052

Dubois, J., & Adolphs, R. (2016). Building a science of individual differences from fMRI. *Trends in cognitive sciences*, *20*(6), 425-443

Fischl, B., Sereno, M. I., Tootell, R. B., & Dale, A. M. (1999). High-resolution intersubject averaging and a coordinate system for the cortical surface. *Human Brain Mapping*, *8*(4), 272–284.

Fukuda, K., Vogel, E., Mayr, U., & Awh, E. (2010). Quantity, not quality: The relationship between fluid intelligence and working memory capacity. *Psychonomic bulletin & review*, *17*, 673-679. https://doi.org/10.3758/17.5.673

Garcea, F. E., Almeida, J., & Mahon, B. Z. (2012). A right visual field advantage for visual processing of manipulable objects. *Cognitive, Affective, & Behavioral Neuroscience*, *12*(4), 813–825. https://doi.org/10.3758/s13415-012-0106-x

Gaser, C., Dahnke, R., Thompson, P. M., Kurth, F., Luders, E., Initiative, A. D. N., & others. (2024). CAT: a computational anatomy toolbox for the analysis of structural MRI data. *Gigascience*, *13*, giae049.

Gayet, S., Guggenmos, M., Christophel, T. B., Haynes, J.-D., Paffen, C. L., Van der Stigchel, S., & Sterzer, P. (2017). Visual working memory enhances the neural response to matching visual input. *Journal of Neuroscience*, *37*(28), 6638–6647.

Genzano, V. R., Di Nocera, F., & Ferlazzo, F. (2001). Upper/lower visual field asymmetry on a spatial relocation memory task: *Neuroreport*, *12*(6), 1227–1230. https://doi.org/10.1097/00001756-200105080-00034

Glasser, M. F., Coalson, T. S., Robinson, E. C., Hacker, C. D., Harwell, J., Yacoub, E., Ugurbil, K., Andersson, J., Beckmann, C. F., Jenkinson, M., Smith, S. M., & Van Essen, D. C. (2016). A multi-modal parcellation of human cerebral cortex. *Nature*, *536*(7615), 171–178. https://doi.org/10.1038/nature18933

Glickstein, M., & Whitteridge, D. (1987). Tatsuji Inouye and the mapping of the visual fields on the human cerebral cortex. *Trends in Neurosciences*, *10*(9), 350–353.

Granziera, C., Daducci, A., Donati, A., Bonnier, G., Romascano, D., Roche, A., Bach Cuadra, M., Schmitter, D., Klöppel, S., Meuli, R., Von Gunten, A., & Krueger, G. (2015). A multi-contrast MRI study of microstructural brain damage in patients with mild cognitive impairment. *NeuroImage: Clinical*, *8*, 631–639. https://doi.org/10.1016/j.nicl.2015.06.003

Gratton, C., Nelson, S. M., & Gordon, E. M. (2022). Brain-behavior correlations: Two paths toward reliability. *Neuron*, *110*(9), 1446-1449.

Hagemeier, J., Tong, O., Dwyer, M. G., Schweser, F., Ramanathan, M., & Zivadinov, R. (2015). Effects of diet on brain iron levels among healthy individuals: An MRI pilot study. *Neurobiology of Aging*, *36*(4), 1678–1685. https://doi.org/10.1016/j.neurobiolaging.2015.01.010

Harrison, S. A., & Tong, F. (2009). Decoding reveals the contents of visual working memory in early visual areas. *Nature*, *458*(7238), 632–635.

Hedge, C., Powell, G., & Sumner, P. (2018). The reliability paradox: Why robust cognitive tasks do not produce reliable individual differences. *Behavior Research Methods*, *50*(3), 1166–1186. https://doi.org/10.3758/s13428-017-0935-1

Himmelberg, M. M., Winawer, J., & Carrasco, M. (2020). Stimulus-dependent contrast sensitivity asymmetries around the visual field. *Journal of Vision*, *20*(9), 18. https://doi.org/10.1167/jov.20.9.18

Himmelberg, M. M., Winawer, J., & Carrasco, M. (2022). Linking individual differences in human primary visual cortex to contrast sensitivity around the visual field. *Nature Communications*, *13*(1), 3309. https://doi.org/10.1038/s41467-022-31041-9

Himmelberg, M. M., Winawer, J., & Carrasco, M. (2023). Polar angle asymmetries in visual perception and neural architecture. *Trends in Neurosciences*, *46*(6), 445–458. https://doi.org/10.1016/j.tins.2023.03.006

Hockey, A., & Geffen, G. (2004). The concurrent validity and test–retest reliability of a visuospatial working memory task. *Intelligence*, *32*(6), 591–605.

Iamshchinina, P., Christophel, T. B., Gayet, S., & Rademaker, R. L. (2021). Essential considerations for exploring visual working memory storage in the human brain. *Visual Cognition*, *29*(7), 425–436. https://doi.org/10.1080/13506285.2021.1915902

Jeong, S. K. (2023). Perceived image size modulates visual memory. *Psychonomic Bulletin & Review, 30*(6), 2282–2288. https://doi.org/10.3758/s13423-023-02280-2

Jerde, T. A., Merriam, E. P., Riggall, A. C., Hedges, J. H., & Curtis, C. E. (2012). Prioritized Maps of Space in Human Frontoparietal Cortex. *The Journal of Neuroscience*, *32*(48), 17382–17390. https://doi.org/10.1523/JNEUROSCI.3810-12.2012

Johnson, M. K., McMahon, R. P., Robinson, B. M., Harvey, A. N., Hahn, B., Leonard, C. J., Luck, S. J., & Gold, J. M. (2013). The relationship between working memory capacity and broad measures of cognitive ability in healthy adults and people with schizophrenia. *Neuropsychology*, *27*(2), 220.

Kang, K., Seidlitz, J., Bethlehem, R. A. I., Xiong, J., Jones, M. T., Mehta, K., Keller, A. S., Tao, R., Randolph, A., Larsen, B., Tervo-Clemmens, B., Feczko, E., Dominguez, O. M., Nelson, S. M., Lifespan Brain Chart Consortium, Alexander-Bloch, A. F., Fair, D. A., Schildcrout, J., Fair, D. A., … Vandekar, S. (2024). Study design features increase replicability in brain-wide association studies. *Nature*, *636*(8043), 719–727. https://doi.org/10.1038/s41586-024-08260-9

Karim, A. K. M. R., & Kojima, H. (2010). The *what* and *why* of perceptual asymmetries in the visual domain. *Advances in Cognitive Psychology*, *6*(1), 103–115. https://doi.org/10.2478/v10053-008-0080-6

Knops, A., Nuerk, H.-C., Fimm, B., Vohn, R., & Willmes, K. (2006). A special role for numbers in working memory? An fMRI study. *Neuroimage*, *29*(1), 1–14.

Konstantinou, N., Constantinidou, F., & Kanai, R. (2017). Discrete capacity limits and neuroanatomical correlates of visual short-term memory for objects and spatial locations. *Human Brain Mapping*, *38*(2), 767–778.

Kurzawski, J. W., Gulban, O. F., Jamison, K., Winawer, J., & Kay, K. (2022). Non-neural factors influencing BOLD response magnitudes within individual subjects. *Journal of Neuroscience*, *42*(38), 7256–7266.

Lefco, R. W., Brissenden, J. A., Noyce, A. L., Tobyne, S. M., & Somers, D. C. (2020). Gradients of functional organization in posterior parietal cortex revealed by visual attention, visual short-term memory, and intrinsic functional connectivity. *NeuroImage*, *219*, 117029. https://doi.org/10.1016/j.neuroimage.2020.117029

Leutritz, T., Seif, M., Helms, G., Samson, R. S., Curt, A., Freund, P., & Weiskopf, N. (2020). Multiparameter mapping of relaxation (R1 , R2 *), proton density and magnetization transfer saturation at 3 T: A multicenter dual‐vendor reproducibility and repeatability study. *Human Brain Mapping*, *41*(15), 4232–4247. https://doi.org/10.1002/hbm.25122

Liu, T., Heeger, D. J., & Carrasco, M. (2006). Neural correlates of the visual vertical meridian asymmetry. *Journal of Vision*, *6*(11), 12–12. https://doi.org/10.1167/6.11.12

Lorenc, E. S., Mallett, R., & Lewis-Peacock, J. A. (2021). Distraction in visual working memory: Resistance is not futile. *Trends in cognitive sciences*, *25*(3), 228-239. https://doi.org/10.1016/j.tics.2020.12.004

Lorio, S., Tierney, T. M., McDowell, A., Arthurs, O. J., Lutti, A., Weiskopf, N., & Carmichael, D. W. (2019). Flexible proton density (PD) mapping using multi-contrast variable flip angle (VFA) data. *NeuroImage*, *186*, 464–475. https://doi.org/10.1016/j.neuroimage.2018.11.023

Lu, X., Huang, J., Yi, Y., Shen, M., Weng, X., & Gao, Z. (2016). Holding biological motion in working memory: An fMRI study. *Frontiers in Human Neuroscience*, *10*, 251.

Luck, S. J., & Vogel, E. K. (2013). Visual working memory capacity: From psychophysics and neurobiology to individual differences. *Trends in Cognitive Sciences*, *17*(8), 391–400.

Ma, W. J., Husain, M., & Bays, P. M. (2014). Changing concepts of working memory. *Nature Neuroscience*, *17*(3), 347–356.

Maldjian, J. A., Laurienti, P. J., Kraft, R. A., & Burdette, J. H. (2003). An automated method for neuroanatomic and cytoarchitectonic atlas-based interrogation of fMRI data sets. *Neuroimage*, *19*(3), 1233–1239.

Marek, S., Tervo-Clemmens, B., Calabro, F. J., Montez, D. F., Kay, B. P., Hatoum, A. S., Donohue, M. R., Foran, W., Miller, R. L., Hendrickson, T. J., *et al.* (2022). Reproducible brain-wide association studies require thousands of individuals. *Nature, 603*(7902), 654–660. https://doi.org/10.1038/s41586-022-04492-9

Mayberg, H. S., Liotti, M., Brannan, S. K., McGinnis, S., Mahurin, R. K., Jerabek, P. A., Silva, J. A., Tekell, J. L., Martin, C. C., Lancaster, J. L., & Fox, P. T. (1999). Reciprocal limbic-cortical function and negative mood: Converging PET findings in depression and normal sadness. In *American Journal of Psychiatry* (Vol. 156, Issue 5, pp. 675–682). https://doi.org/10.1176/ajp.156.5.675

Miller, E. K., Erickson, C. A., & Desimone, R. (1996). Neural mechanisms of visual working memory in prefrontal cortex of the macaque. *Journal of Neuroscience*, *16*(16), 5154–5167.

Montaser-Kouhsari, L., & Carrasco, M. (2009). Perceptual asymmetries are preserved in short-term memory tasks. *Attention, Perception & Psychophysics*, *71*(8), 1782–1792. https://doi.org/10.3758/APP.71.8.1782

Nieuwenhuis, S., Forstmann, B. U., & Wagenmakers, E.-J. (2011). Erroneous analyses of interactions in neuroscience: A problem of significance. *Nature Neuroscience*, *14*(9), 1105–1107. https://doi.org/10.1038/nn.2886

O'Connell, C., Ho, L. C., Murphy, M. C., Conner, I. P., Wollstein, G., Cham, R., & Chan, K. C. (2016). Structural and functional correlates of visual field asymmetry in the human brain by diffusion kurtosis MRI and functional MRI. *Neuroreport*, *27*(16), 1225–1231.

Offen, S., Gardner, J. L., Schluppeck, D., & Heeger, D. J. (2010). Differential roles for frontal eye fields (FEFs) and intraparietal sulcus (IPS) in visual working memory and visual attention. *Journal of Vision*, *10*(11), 28–28. https://doi.org/10.1167/10.11.28

Peirce, J., Gray, J. R., Simpson, S., MacAskill, M., Höchenberger, R., Sogo, H., Kastman, E., & Lindeløv, J. K. (2019). PsychoPy2: Experiments in behavior made easy. *Behavior Research Methods*, *51*(1), 195–203. https://doi.org/10.3758/s13428-018-01193-y

Pirpamer, L., Hofer, E., Gesierich, B., De Guio, F., Freudenberger, P., Seiler, S., Duering, M., Jouvent, E., Duchesnay, E., Dichgans, M., Ropele, S., & Schmidt, R. (2016). Determinants of iron accumulation in the normal aging brain. *Neurobiology of Aging*, *43*, 149–155. https://doi.org/10.1016/j.neurobiolaging.2016.04.002

Purokayastha, S., Roberts, M., & Carrasco, M. (2021). Voluntary attention improves performance similarly around the visual field. *Attention, Perception, & Psychophysics*, *83*(7), 2784–2794. https://doi.org/10.3758/s13414-021-02316-y

R Core Team. (2023). *R: A Language and Environment for Statistical Computing* [Computer software]. . R Foundation for Statistical Computing. https://www.R-project.org

Raven, E. P., Lu, P. H., Tishler, T. A., Heydari, P., & Bartzokis, G. (2013). Increased iron levels and decreased tissue integrity in hippocampus of Alzheimer's disease detected in vivo with magnetic resonance imaging. *Journal of Alzheimer's Disease*, *37*(1), 127–136.

Rezec, A., & Dobkins, K. (2004). Attentional weighting: A possible account of visual field asymmetries in visual search? *Spatial Vision*, *17*(4), 269–293. https://doi.org/10.1163/1568568041920203

Rosenberg, M. D., & Finn, E. S. (2022). How to establish robust brain–behavior relationships without thousands of individuals. *Nature neuroscience*, *25*(7), 835-837.

Rossion, B., & Pourtois, G. (2004). Revisiting Snodgrass and Vanderwart's Object Pictorial Set: The Role of Surface Detail in Basic-Level Object Recognition. Perception, 33(2), 217–236. https://doi.org/10.1068/p5117.

Schneiders, J. A., Opitz, B., Krick, C. M., & Mecklinger, A. (2011). Separating intra-modal and across-modal training effects in visual working memory: An fMRI investigation. *Cerebral Cortex*, *21*(11), 2555–2564.

Serences, J. T., Ester, E. F., Vogel, E. K., & Awh, E. (2009). Stimulus-specific delay activity in human primary visual cortex. *Psychological Science*, *20*(2), 207–214.

Sereno, M. I., Dale, A. M., Reppas, J. B., Kwong, K. K., Belliveau, J. W., Brady, T. J., Rosen, B. R., & Tootell, R. B. (1995). Borders of multiple visual areas in humans revealed by functional magnetic resonance imaging. *Science*, *268*(5212), 889–893.

Sheremata, S., Malcolm, G. L., & Shomstein, S. (2023). Behavioral asymmetries in visual short-term memory occur in retinotopic coordinates. *Attention, Perception, & Psychophysics*, *85*(1), 113–119. https://doi.org/10.3758/s13414-022-02610-3

Snodgrass, J. G., & Vanderwart, M. (1980). A standardized set of 260 pictures: Norms for name agreement, image agreement, familiarity, and visual complexity. *Journal of Experimental Psychology: Human Learning and Memory*, *6*(2), 174–215. https://doi.org/10.1037/0278-7393.6.2.174

Song, H., Chui, T. Y. P., Zhong, Z., Elsner, A. E., & Burns, S. A. (2011). Variation of cone photoreceptor packing density with retinal eccentricity and age. *Investigative Ophthalmology & Visual Science*, *52*(10), 7376–7384.

Spence, H., McNeil, C. J., & Waiter, G. D. (2020). The impact of brain iron accumulation on cognition: A systematic review. *PLOS ONE*, *15*(10), e0240697. https://doi.org/10.1371/journal.pone.0240697

Strong, R. W., & Alvarez, G. A. (2020). Hemifield-specific control of spatial attention and working memory: Evidence from hemifield crossover costs. *Journal of Vision*, *20*(8), 24. https://doi.org/10.1167/jov.20.8.24

Sudheimer, K., Keller, J., Gomez, R., Tennakoon, L., Reiss, A., Garrett, A., Kenna, H., O'hara, R., & Schatzberg, A. F. (2015). Decreased hypothalamic functional connectivity with subgenual cortex in psychotic major depression. *Neuropsychopharmacology*, *40*(4), 849–860.

Tabelow, K., Balteau, E., Ashburner, J., Callaghan, M. F., Draganski, B., Helms, G., Kherif, F., Leutritz, T., Lutti, A., Phillips, C., Reimer, E., Ruthotto, L., Seif, M., Weiskopf, N., Ziegler, G., & Mohammadi, S. (2019). hMRI – A toolbox for quantitative MRI in neuroscience and clinical research. *NeuroImage*, *194*, 191–210. https://doi.org/10.1016/j.neuroimage.2019.01.029

Tardiff, N., & Curtis, C. E. (2025). *Short-term and working memory*. In J. H. Byrne (Ed.), *Learning and memory: A comprehensive reference* (3rd ed., pp. 112–133). Elsevier. https://doi.org/10.1016/B978-0-443-15754-7.00025-0

Thaler, L., Schütz, A. C., Goodale, M. A., & Gegenfurtner, K. R. (2013). What is the best fixation target? The effect of target shape on stability of fixational eye movements. *Vision Research*, *76*, 31–42. https://doi.org/10.1016/j.visres.2012.10.012

Torchiano, M. & others. (2020). *effsize: Efficient effect size computation*.

Wallis, C. U., Cardinal, R. N., Alexander, L., Roberts, A. C., & Clarke, H. F. (2017). Opposing roles of primate areas 25 and 32 and their putative rodent homologs in the regulation of negative emotion. *Proceedings of the National Academy of Sciences*, *114*(20), E4075–E4084.

Watson, A. B. (2014). A formula for human retinal ganglion cell receptive field density as a function of visual field location. *Journal of Vision*, *14*(7), 15–15.

Weiskopf, N., Suckling, J., Williams, G., Correia, M. M., Inkster, B., Tait, R., Ooi, C., Bullmore, E. T., & Lutti, A. (2013). Quantitative multi-parameter mapping of R1, PD*, MT, and R2* at 3T: a multi-center validation. *Frontiers in Neuroscience*, *7*, 95.

Wellcome Trust Centre for Neuroimaging. (2014). *SPM12*. University College London. https://www.fil.ion.ucl.ac.uk/spm/software/spm12/

Wenger, E., Polk, S. E., Kleemeyer, M. M., Weiskopf, N., Bodammer, N. C., Lindenberger, U., & Brandmaier, A. M. (2022). Reliability of quantitative multiparameter maps is high for magnetization transfer and proton density but attenuated for R_1 and R_2* in healthy young adults. *Human Brain Mapping*, *43*(11), 3585–3603. https://doi.org/10.1002/hbm.25870

Wickham, H. (2007). Reshaping data with the reshape package. *Journal of Statistical Software*, *21*(12). https://www.jstatsoft.org/v21/i12/

Wickham, H., Averick, M., Bryan, J., Chang, W., McGowan, L. D., François, R., Grolemund, G., Hayes, A., Henry, L., Hester, J., Kuhn, M., Pedersen, T. L., Miller, E., Bache, S. M., Müller, K., Ooms, J., Robinson, D., Seidel, D. P., Spinu, V., … Yutani, H. (2019). Welcome to the Tidyverse. *Journal of Open Source Software*, *4*(43), 1686. https://doi.org/10.21105/joss.01686

Xiao, Y., Lin, Y., Ma, J., Qian, J., Ke, Z., Li, L., Yi, Y., Zhang, J., Cam-CAN, & Dai, Z. (2021). Predicting visual working memory with multimodal magnetic resonance imaging. *Human Brain Mapping, 42*(5), 1446–1462. https://doi.org/10.1002/hbm.25305

Zhang, Y., Ye, C., Roberson, D., Zhao, G., Xue, C., & Liu, Q. (2017). The Bilateral Field Advantage Effect in Memory Precision. *Quarterly Journal of Experimental Psychology*, 17470218.2016.1. https://doi.org/10.1080/17470218.2016.1276943

Zhao, Y.-J., Kay, K. N., Tian, Y., & Ku, Y. (2022). Sensory Recruitment Revisited: Ipsilateral V1 Involved in Visual Working Memory. *Cerebral Cortex*, *32*(7), 1470–1479. https://doi.org/10.1093/cercor/bhab300

Zito, G. A., Cazzoli, D., Müri, R. M., Mosimann, U. P., & Nef, T. (2016). Behavioral Differences in the Upper and Lower Visual Hemifields in Shape and Motion Perception. *Frontiers in Behavioral Neuroscience*, *10*. https://doi.org/10.3389/fnbeh.2016.00128